Biosensors and Bioelectronics 55 (2014) 57–65

Contents lists available at ScienceDirect

Biosensors and Bioelectronics

journal homepage: www.elsevier.com/locate/bios

Inducing electrocatalytic functionality in ZnO thin film by N doping to realize a third generation uric acid biosensor

Kajal Jindal [a], Monika Tomar [b], Vinay Gupta [a,*]

[a] Department of Physics and Astrophysics, University of Delhi, Delhi 110007, India
[b] Department of Physics, Miranda House, University of Delhi, Delhi 110007, India

ARTICLE INFO

Article history:
Received 8 August 2013
Received in revised form
4 November 2013
Accepted 5 November 2013
Available online 1 December 2013

Keywords:
Uric acid
Zinc oxide
Nitrogen
Pulsed laser deposition
Third generation biosensor

ABSTRACT

A third generation uric acid biosensor has been developed by exploiting the electrocatalytic functionality of nitrogen (N) doped zinc oxide (ZnO:N) thin film matrix deposited using pulsed laser deposition technique. The electrochemistry of ZnO:N thin film based electrode is investigated by using electrochemical impedance spectroscopy and cyclic voltammetry. The obtained results demonstrate that nitrogen doping in ZnO matrix offers a striking electrocatalytic activity to the immobilized uricase towards the oxidation of analyte (uric acid) and promotes the direct transfer of electrons from active sites of enzyme onto the electrode without any mediator. In contrast to pure ZnO, ZnO:N (8% N) thin film based uric acid biosensor gives a high sensitivity of about 1.38 mA/mM in the absence of mediator. Moreover, ZnO:N derived bio-electrode exhibits excellent selectivity and outstanding analytical stability and reproducibility, which enables a reliable and sensitive determination of uric acid in the serum. The ZnO:N thin film based biosensor exhibits a linear sensing response in the range from 0 to 1.0 mM of uric acid concentration and the apparent Michaelis–Menten kinetic parameter (*Km*) is estimated to be about 0.13 mM which indicates the high affinity of the prepared bio-electrode towards uric acid. The obtained results are encouraging and indicate that the ZnO:N thin film matrix offers a new and promising platform for the development of novel third generation biosensors without using any mediator.

1. Introduction

Uric acid is the end metabolic product of purine through the liver and is a chief nitrogenous component of biological fluids such as urine and blood serum. Its presence in human blood above a tolerable level (0.13–0.46 mM) is an indicator of several diseases such as gout, hyperuricemia or Lesch-Nyhan syndrome, arthritis, diabetes, high cholesterol, cardiovascular and kidney diseases (Zhang et al., 2007). Thus, quantification of uric acid level in blood is of significant interest for biomedical applications and requires special attention. Many reports are available in literature on the detection of uric acid but hardly any effort is made towards the development of third generation uric acid biosensor which is a key step towards the realization of an integrated biosensor chip (Yin et al., 2009).

Zinc oxide (ZnO) is a technologically important material having multifunctional applications on account of its promising elasto-optic (Dominici et al., 2012), piezoelectric (Tomar et al., 2005), photoconducting (Yadav and Gupta, 2012), and optical wave guiding properties (Mehan et al., 2004). In addition, ZnO has attracted enormous interest over the past few years for biosensing applications for the detection of various biomolecules such as glucose, cholesterol, DNA, H_2O_2 etc. due to good biocompatibility, high stability and presence of native defects such as zinc interstitials and oxygen vacancies (Saha and Gupta 2011; Batra et al., 2012; Das et al., 2010). However, low conductivity and limited charge communication feature restricted the application of ZnO (Arora et al., 2011) for third generation biosensors. For realization of third generation biosensor, system must be free from all kinds of redox mediators and have direct electron transfer capability from the enzyme's active sites onto the electrode (Pundir et al., 2011). The direct electrochemistry may be achieved by identifying a suitable conducting matrix that can connect the active center of redox enzymes with the surface of electrode, or developing a matrix that can directly reach into the active center of enzymes (Cao et al., 2008) and led to the immediate need to tailor the electronic properties of ZnO for introduction of electrocatalytic functionality. Some efforts have been made to introduce redox species in the ZnO based electrodes by doping the redox mediator (Saha et al., 2009). Although, the mediator doped ZnO based system was devoid of free diffusing mediators in the electrolyte solution but the electron transfer process was not direct and was through the shuttling of electrons via mediating species present in

* Corresponding author. Tel.: +91 9811563101.
E-mail addresses: drguptavinay@gmail.com, drvin_gupta@rediffmail.com (V. Gupta).

0956-5663/$ - see front matter © 2013 Elsevier B.V. All rights reserved.
http://dx.doi.org/10.1016/j.bios.2013.11.015

the electrode itself (Saha et al., 2009). Another attempt in this direction has been made by preparing ZnO nanostructures such as nanotubes, nanorods etc. which provides improved catalysis, high surface area and accelerated electron transfer process. But, in all the reports based on possible direct electron transfer via nanostructured ZnO matrix, synthesis has been carried out using chemical route that lead to the development of bio-electrodes with low chemical stability and reproducibility, and thus exhibits a fast decay in the sensing response with time (Fatemi et al., 2012; Ahmad et al., 2012; Kong et al., 2009; Dai et al., 2009; Lu et al., 2008; Zhang et al., 2004). Recently, organic–inorganic hybrid composites have emerged as promising materials for biosensing applications as they effectively integrates the physicochemical attributes of individual components. Extensive efforts are being made to prepare hybrid composites of ZnO with polymers, CNTs and metal nanoparticles (Wang et al., 2012; Wei et al., 2010; Xiang et al., 2009; Wang et al., 2010; Zhang et al., 2010; Devi et al., 2011; Yadav et al., 2011) which results in direct electron transfer and exhibits improved sensitivity as compared to pure ZnO matrix. But, the application is still limited due to the cumbersome fabrication of bio-electrode that involves multiple fabrication steps and large turnaround time which makes them unsuitable for mass production. Thus, it is a growing requirement to develop new materials that can overcome the limitations observed in the previously developed bio-electrodes.

Since, chemical doping is the most effective method for the development of single phase materials; surprisingly, no efforts are being made to intrinsically modify the electronic properties of ZnO by doping with suitable element in order to induce electrocatalytic functionality and facilitate the direct electron transfer feature. Nitrogen is a well known dopant and has been proved to modify the magnetic and electronic properties of ZnO (Jindal et al., 2012; Liu et al., 2012). Although N doping has been exploited well for introducing various functionalities in ZnO but no attention has been paid towards the realization of third generation biosensor despite the fact that introduction of N at O site in ZnO affect the defect profile of ZnO significantly and may introduce the electrocatalytic properties for direct transfer of electrons.

In this paper, we report the development of third generation uric acid biosensor using N doped ZnO (ZnO:N) thin film prepared by pulsed laser deposition (PLD) technique by inducing the high catalytic activity towards the oxidation of uric acid. The prepared ZnO:N thin film matrix allows direct transfer of electron without any mediating species and bio-electrode exhibit high sensitivity, excellent reproducibility and remarkable stability for uric acid.

2. Experimental

Pure zinc oxide (ZnO) and N doped ZnO (ZnO:N) thin films were grown by pulsed laser deposition (PLD) technique using the fourth harmonic of Nd:YAG laser (λ=266 nm). N doping was achieved by mixing Zn_3N_2 powder (99.99% pure) with ZnO powder (99.99% pure) in different proportions in order to prepare one inch dia. $ZnO_{1-x}N_x$ ceramic targets with variable N doping concentrations (x=0, 0.02, 0.04, 0.08 and 0.10). ZnO:N thin films were deposited onto ITO coated glass substrates (commercially available) by ablating the respective ceramic target in oxygen ambient at a growth pressure of 1 mTorr with a fluence of 1.2 J/cm^2 and a repetition rate of 10 Hz. Deposition of thin films was carried out at room temperature substrate and target to substrate distance was maintained at 5 cm. Number of applied laser pulses were controlled in order to maintain the thickness of ZnO and ZnO:N thin films to be fixed at about 60 nm. The electrode based on pure ZnO and ZnO:N thin films having 2%, 4%, 8% and 10% N are referred as ZnO:N (00), ZnO:N (02), ZnO:N (04), ZnO:N (08) and ZnO:N (10) respectively.

In order to prepare the bio-electrode, 10 μl (0.049 U) of the freshly prepared uricase solution (1 mg/ml in PBS solution) is drop casted on the surface of ZnO:N(x)/ITO/glass electrode so as to immobilize uricase electrostatically via physical adsorption technique as shown in Scheme 1.

Details of the various reagents (enzyme solutions and analyte concentrations), fabrication of bio-electrode, materials characterization techniques and electrochemical characterization are given in Supplementary information.

3. Results and discussion

3.1. Characterization of ZnO and ZnO:N thin films

3.1.1. Structural studies using XRD

All ZnO and ZnO:N(x) thin films prepared by pulsed laser deposition technique were found to be smooth, transparent and strongly adherent to the ITO/glass substrate. Supplementary Fig. 1 displays the XRD spectra of the as-deposited ZnO and ZnO:N thin films as a function of N doping concentration from 0 to 10 at %. It may be noted from Supplementary Fig. 1 that all the prepared thin films exhibit well defined reflection corresponding to (002) plane of the wurtzite structure of ZnO indicating the growth of preferred oriented film with the c-axis normal to the substrate (Gupta and Mansingh, 1996). No other peaks are being observed in the XRD spectra of all deposited thin films which demonstrate the formation of single phase material (Supplementary Fig. 1). Pure ZnO thin film exhibits (002) diffraction peak at $2\theta \approx 34.30^\circ$ which is close to the corresponding value reported for bulk ZnO (34.43°) (Mehan et al., 2004). A slight shift in the (002) diffraction peak is observed towards lower angles with increasing N doping concentration

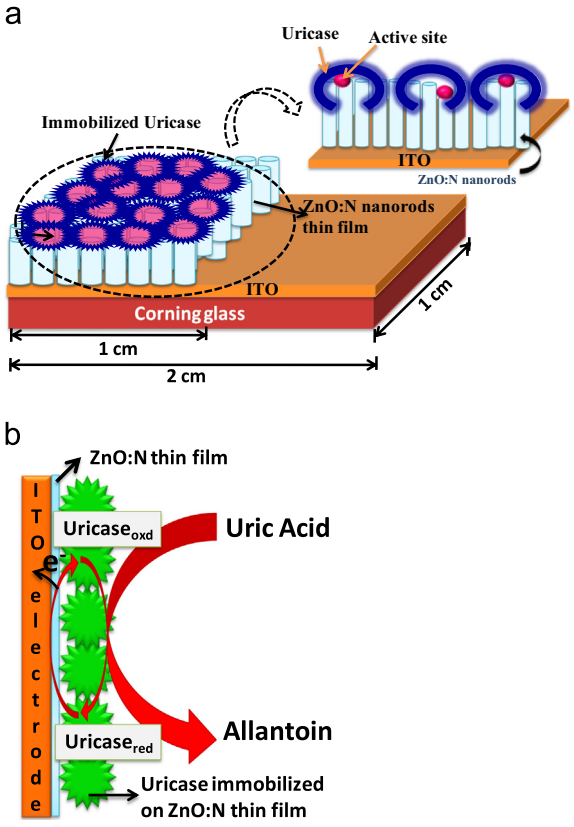

Scheme 1. (a) Schematic representation of linkage of enzyme active site to the electrode for direct electron transfer (b) Schematic of the electron exchange occurring in the developed ZnO:N thin film based third generation uric acid biosensor.

(Supplementary Fig. 1). This may be due to the fact that N has slightly larger ionic radii (1.46 Å) in comparison to that of O (1.40 Å) which upon incorporation in the ZnO host lattice at O sites results in an expansion in the lattice along c-axis and thus leads to a shift in (002) XRD peak towards lower angles.

3.1.2. Vibrational properties using Raman spectroscopy

Raman scattering studies were performed in order to identify the incorporation of N^{3-} ions into ZnO host lattice. The Raman spectrum was recorded in the back scattering configuration where the direction of incident light is parallel to the *c*-axis growth direction of the deposited ZnO:N thin films and the scattered light is detected in the opposite direction. Room temperature Raman spectra of prepared ZnO and ZnO:N thin films are shown in Fig. 1. The Raman spectra (Fig. 1) show characteristic modes [E_2(low) and E_2(high)] corresponding to wurtzite structure of ZnO and A_1(LO) and E_1(LO) corresponding to disorder in the lattice (Yadav et al., 2012). The pure ZnO thin film exhibits E_2(low) and E_2(high) phonon modes at 99.0 cm^{-1} and 438.5 cm^{-1} respectively and the values are close to the ones reported for ZnO thin films deposited by other techniques (Yadav et al., 2007). It may be observed from the Raman spectra (Fig. 1) that E_2 (high) mode, which is associated with the vibration of O sublattice, shows a shift towards lower frequencies (red shift) with increase in N doping concentration in ZnO. This may be attributed to the stress induced by incorporation of N^{3-} at O^{2-} sites in ZnO lattice which results in an expansion in the unit cell and confirms the substitution of N at O sites in ZnO host lattice. It is important to note from Fig. 1 that an additional mode at 275 cm^{-1} is observed for all ZnO:N thin films and intensity of this mode increases with increase in the concentration of N dopant in ZnO. The phonon mode at 275 cm^{-1} has been reported to arise as a result of the formation of complexes between Zn interstitials and nitrogen (Zn_i–N_O) (Wu et al., 2012). Therefore, the appearance of additional mode at 275 cm^{-1} in ZnO:N thin films indicate that defects in the form of Zn interstitial arise in the ZnO as a result of increasing N doping concentration and being donor defects alter the electronic properties of ZnO. Another phonon mode at 510 cm^{-1} (Fig. 1) is also observed in ZnO:N thin film samples and is attributed to the formation of complexes between Zn interstitial and O interstitial (Zn_i–O_i) due to nitrogen doping (Game et al., 2012). Therefore incorporation of N influences the defect profile of ZnO significantly, which may play a crucial role in governing the biosensing response characteristics.

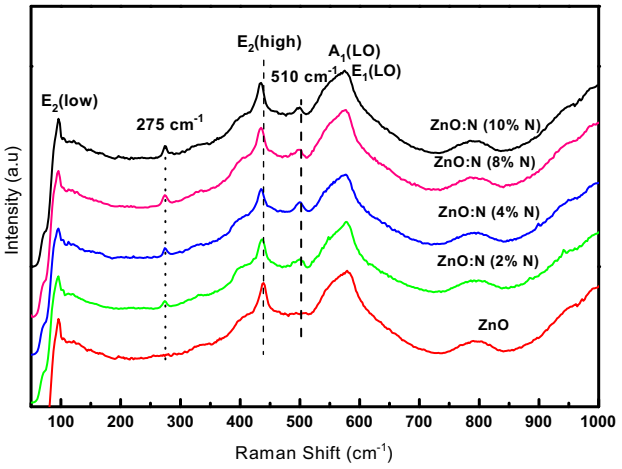

Fig. 1. Raman spectra of the ZnO and nitrogen doped ZnO (ZnO:N) thin films prepared by pulsed laser deposition technique.

3.1.3. Optical studies

Photoluminescence (PL) measurement is the most powerful tool in order to identify the induced disorder and defects in the host lattice of a material as a result of doping. The PL spectra of the prepared ZnO and ZnO:N thin films is investigated at room temperature and is shown in Fig. 2. It may be seen from Fig. 2 that a broad and well defined near band edge (NBE) emission peak originating from the recombination of free exciton is observed in all deposited ZnO and ZnO:N thin films. Pure ZnO thin film exhibits NBE peak at around 3.12 eV which is close to the corresponding reported value (Saha and Gupta 2011). A red shift

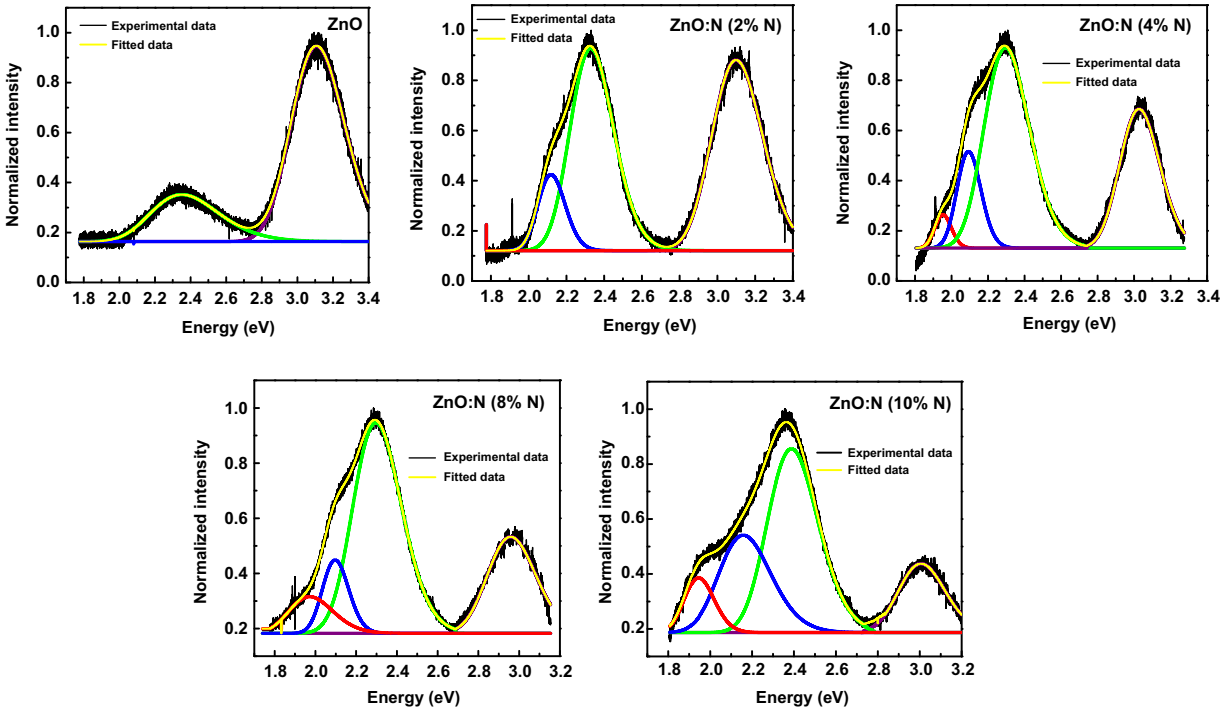

Fig. 2. Room temperature PL spectra of the ZnO and ZnO:N thin films prepared by pulsed laser deposition technique.

in the NBE peak from 3.12 eV to 2.95 eV is observed (Fig. 2) with increasing N doping concentration in ZnO from 0 to 10%. This is attributed to a decrease in the band gap of ZnO as a result of N doping due to the mixing of O 2p and N 2p orbitals which leads to more available states in the band gap (Jindal et al., 2012). Another broad emission peak is also observed around 2.3 eV in the PL spectra of all prepared samples (Fig. 2), which is associated with the presence of deep level structural defects in ZnO lattice (Zeng et al., 2010). It may be clearly seen from Fig. 2 that ratio of intensities of NBE to that of deep level defects emission decreases continuously with increase in the concentration of N doping in ZnO upto 10% suggesting an increase in the defects in the ZnO film with incorporation of N. The emission peak corresponding to deep level defects has been deconvoluted by fitting Gaussian curves. The defect emission peak (Fig. 2) is found to be constituted of multiple peaks corresponding to green emission due to singly charged oxygen vacancies (V_O^+) at about 2.33 eV (Zeng et al., 2010; Panigrahy et al., 2010), Zn antisites (Zn_O) defect emission at about 2.11 eV (Wu et al., 2010) and another peak at 1.98 eV which has been reported to arise as a result of yellow emission due to presence of interstitial oxygen (O_i) (Panigrahy et al., 2010; Djurišić et al., 2006). Fig. 2 demonstrates that only defects corresponding to oxygen vacancies (V_O) are being observed in pure ZnO thin films and it is important to point out that N incorporation in ZnO (ZnO:N, 2% N) leads to an increase in the defects due to oxygen vacancies (V_O). The defects due to Zn antisites are not observed in pure ZnO and arise on doping ZnO with N. Also, the intensity of yellow emission peak was found to increase for ZnO:N thin films having higher N dopant concentration and is in agreement to the Raman studies which demonstrated an increase in O interstitials defects in ZnO with introduction of N dopant. These native defects in ZnO:N thin film play a crucial role in altering its charge transfer characteristics.

3.2. Electrochemical studies

3.2.1. Electrochemical impedance spectroscopy

To further study the role of N doping in ZnO, the electron transfer capability of the prepared electrodes was monitored by electrochemical impedance spectroscopy (EIS). The EIS spectra shows a Nyquist plot having a semicircular part at higher frequencies corresponding to the electron transfer-limited process and its diameter is equal to the electron transfer resistance (*Rct*), which controls the electron transfer kinetics of the redox probe at the electrode interface (Niu et al., 2009). EIS spectra of ZnO:N (00), ZnO:N (02), ZnO:N (04), ZnO:N (08) and ZnO:N (10) electrodes were recorded in the presence of redox probe $[Fe(CN)_6]^{3-/4-}$ and are shown in Fig. 3(a). The value of *Rct* for the pure ZnO thin film matrix is found to be about 1.4 kΩ which suggests that the surface of ZnO thin film matrix is providing some hindrance to the transfer of electrons. However, it may be seen that the value of *Rct* reduces significantly with introduction of N dopant in ZnO matrix, and

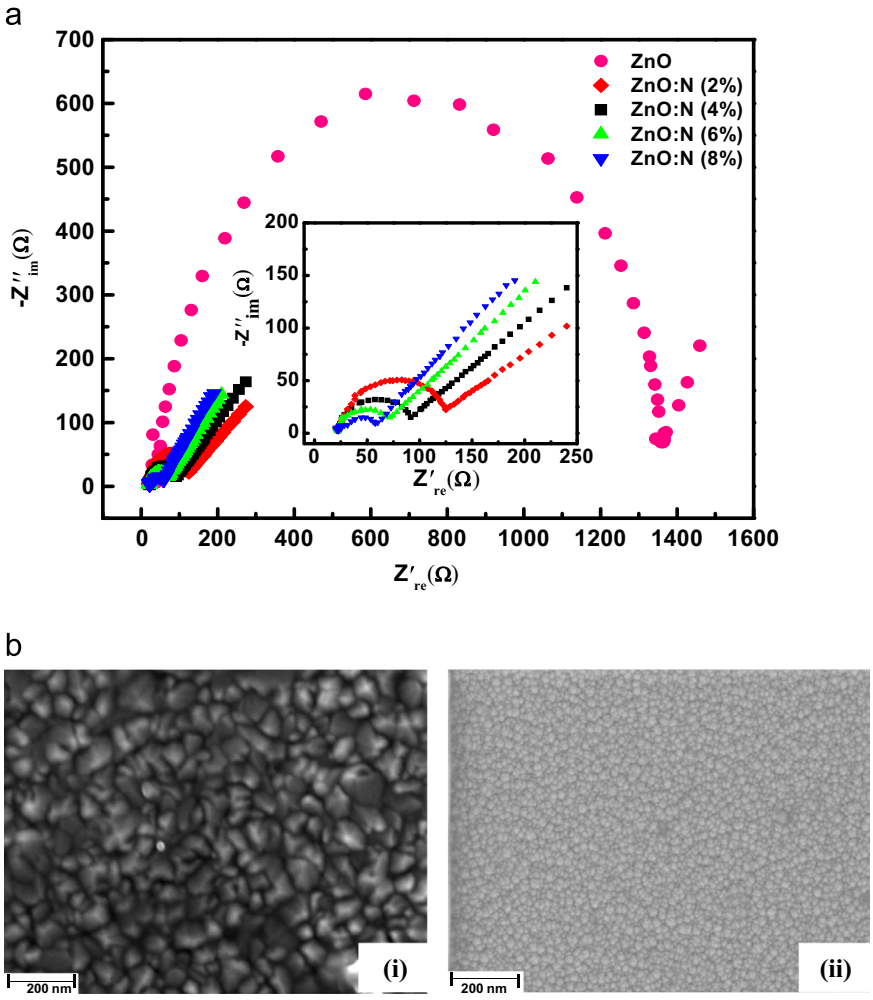

Fig. 3. (a) EIS spectra of the prepared ZnO and ZnO:N thin films recorded in the presence of redox probe $[Fe(CN)_6]^{3-/4-}$. Inset gives the enlarged version of the image demonstrating the change in *Rct* as a result of N doping in ZnO. (b) SEM image of the (i) ZnO:N nanorod (ZnO:N(08)) thin film grown on ITO/glass electrode (ii) ZnO:N thin film grown at 500 °C substrate temperature on ITO/glass electrode (Matrix B).

decreases continuously from 100 Ω to 30 Ω with increase in the value of N doping from 2 to 8% (inset of Fig. 3(a)) exhibiting a minimum *Rct* of about 30 Ω for the ZnO:N (08) thin film based electrode. This low value of *Rct* may be attributed to the fact that N doping in ZnO introduces free charge carriers by inducing the native defects (V_O, Zn_O, O_i as seen in Figs. 1 and 2) in the prepared ZnO:N thin film and offers a conductive matrix which connects active sites of redox enzyme (uricase) and the electrode, thereby, accelerating the electron transfer process for possible development of third generation biosensor. The *Rct* value further increases for ZnO:N (10) thin film based electrode indicating that the high N doping hinders the electron transfer capability. It may be noted that the obtained value of *Rct* for ZnO:N(08) thin film is much smaller than that of undoped ZnO thin film which clearly indicates that 8% N doped ZnO thin film matrix is optimum and provides efficient electron conduction channel between the electrode and enzyme.

3.3. Immobilization of uricase onto ZnO:N thin film matrix

3.3.1. Surface morphology of the ZnO:N thin film based electrode

The surface morphology of as deposited ZnO:N thin film before and after enzyme immobilization is investigated using an atomic force microscopy (AFM) and the typical micro-images are shown in Supplementary Fig. 2a and b respectively for ZnO:N(08) film. AFM image of the ZnO:N thin film shows a rough surface morphology with uniformly distributed grains which is beneficial for efficient loading of enzyme on its surface. Upon immobilizing the uricase on the surface of ZnO:N thin film, clusters of uricase bio-molecules forming a globular structure of much bigger size may be seen in Supplementary Fig. 2b. This confirms the successful immobilization of enzyme (uricase) onto the surface of ZnO:N (08) thin film electrode. The average root mean square (rms) roughness of the surface of ZnO:N(08) thin film is found to increase from 11 nm to 30 nm after the immobilization of uricase.

3.3.2. FTIR studies

The prepared ZnO:N(08) thin film was characterized by FTIR spectroscopy in the range of 400–4000 cm^{-1} before and after immobilization of uricase enzyme and the corresponding spectra are shown in Supplementary Fig. 3a and b respectively. The IR spectrum of ZnO:N thin film shows the characteristic absorption bands of ZnO at 457 and 567 cm^{-1} (Supplementary Fig. 3a) which originates from the stretching mode of Zn–O bond and confirms that N is substituting well at the O lattice sites in wurtzite structure of ZnO (Menon et al., 2011). The binding of the enzyme (uricase) onto the surface of ZnO:N(08) thin film electrode is revealed by the appearance of additional absorption bands at 985, 1086, 1644, 2386 and 3375 cm^{-1} (Supplementary Fig. 3b). The mode at 1644 cm^{-1} is associated with the C–O stretching vibration of amide I group present in uricase enzyme (Lu et al., 2008). The absorption bands at 985 cm^{-1} and 1086 cm^{-1} corresponds to =C–H in-plane vibrations (Devi et al., 2011) in the immobilized enzyme. Furthermore, a broad absorption peak at around 2386 cm^{-1} and 3375 cm^{-1} are related to the O–H stretching mode (Guo et al., 2012). The observed absorption modes confirms the effective immobilization of uricase onto the surface of ZnO:N thin film matrix.

3.4. Cyclic voltammetry

The cyclic voltammetric (CV) measurements on ITO/glass, ZnO/ITO/glass and ZnO:N(*x*)/ITO/glass electrodes were recorded on immobilization with uricase. The measurements were carried out in 50 mM PBS (pH 7.0) without any mediator by continuously cycling the electrode potential between −0.4 V and +0.3 V with respect to Ag/AgCl as reference electrode at a potential scan rate of 100 mV/s and the obtained CV spectra are shown in Fig. 4(a). It may be seen from Fig. 4(a) that pure ZnO thin film based electrode does not exhibit any redox peak in the entire measured range of sweep voltage. The observed results clearly indicates that ZnO is not electrochemically active in the measured potential window which may be due to the fact that active sites of enzyme are shielded by insulating protein shells and the ZnO thin film does not provide suitable conformation to the immobilized uricase enzyme for the direct transfer of electrons onto the electrode. However, a well-defined and enhanced oxidation and reduction peaks are observed in a PBS buffer without any mediator corresponding to the redox of immobilized uricase on the surface of N doped ZnO thin films (Fig. 4(a)). Since, N doping is observed to be a key parameter to tune the defect profile of ZnO thin film matrix for biosensing response characteristics, the concentration of N dopant in ZnO has been optimized. It may be observed from Fig. 4(a) that the magnitude of oxidation and reduction peak current increases with increase in N doping concentration from 2 to 8% in ZnO. This increase may be understood from the fact that N doping in ZnO

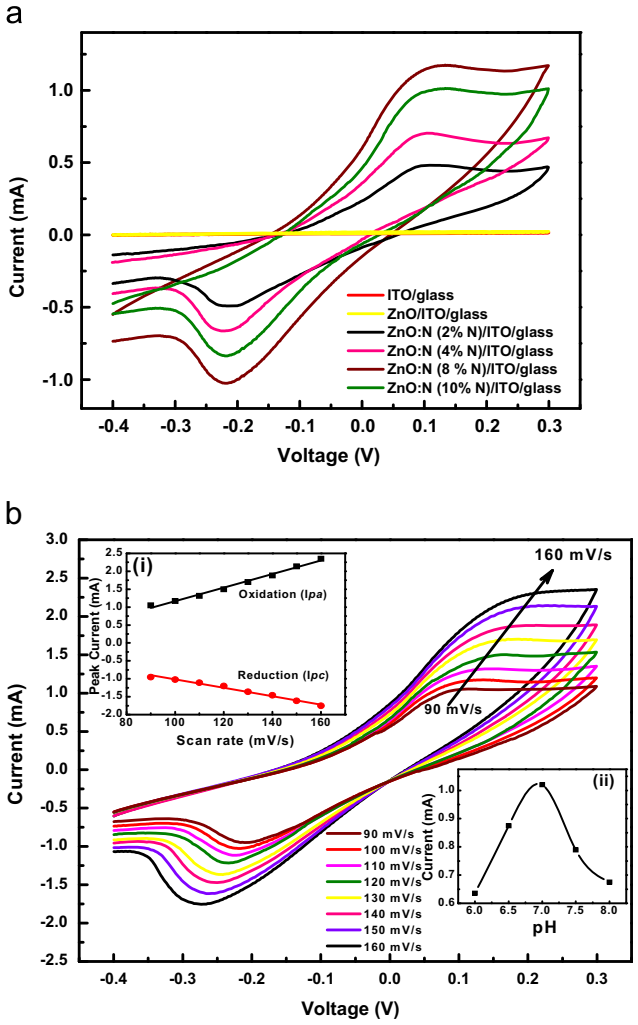

Fig. 4. (a) CV spectra of the ZnO and ZnO:N thin films based electrode as a function of N doping concentration on immobilization of uricase; (b) CV spectra of Uricase/ZnO:N(08)/ITO/glass bio-electrode in PBS solution (without mediator) as a function of scan rate varied from 90 to 160 mV/s. Inset (i) gives the variation in anodic (*Ipa*) and cathodic peak currents (*Ipc*) as a function of scan rate and inset (ii) gives the variation in peak oxidation current with pH of PBS buffer.

host lattice induces structural defects (V_O, Zn_O, O_i as seen in Fig. 2) in the prepared thin film and provides suitable conformation to the enzyme which facilitates the direct electron transfer from the deep buried enzyme electroactive sites to the electrode. This highlights the superior electrocatalytic activity of N doped ZnO thin film matrix in contrast to that of pure ZnO. However, on further increasing the N doping concentration to 10% in ZnO, a slight decrease in the peak oxidation currents is observed (Fig. 4(a)). This decrease may be due to the fact that when N doping concentration is increased to 10%, it no longer occupy oxygen sites in ZnO lattice and instead tends to move towards interstitial positions where it combines with other interstitial N to form N_2 which hinder the transfer of charge carriers (Li et al., 2012; Gao et al., 2010). Thus, the optimum N doping concentration in ZnO thin film is chosen to be 8% and the resulting N doped ZnO [ZnO:N(08)] thin film electrode is employed to investigate the electrocatalytic properties towards oxidation of uric acid. The obtained results are in agreement to the EIS studies discussed earlier. Therefore, further studies related to biosensing response were carried out on ZnO:N(08) electrode only. It may be noted from EIS spectra that N doping improves the electrical conductivity of ZnO by creating defects. Thus, in the present work, deposition conditions of prepared ZnO:N matrix are being optimized so that the grown ZnO:N thin films are electrically conducting in contrast to pure ZnO and the thickness of ZnO:N thin film is also kept to be small (60 nm) in order to facilitate the direct electron transfer for fabrication of third generation biosensor.

A control experiment was carried out in order to examine the electrocatalytic behavior of N doped ZnO [ZnO:N(08)] thin film and thus, a CV spectra were recorded for the ZnO:N(08) thin film electrodes in PBS solution without immobilizing uricase. It is worthwhile to note that the CV spectra did not give any redox peaks at any measured potential and thus points towards the fact that the observed electrocatalytic behavior is solely due to the direct electrochemistry of uricase immobilized on the ZnO:N thin film.

Uricase (Urate oxidase) is a 135 kDa tunnel-shaped homotetramer with four subunits assembled *via* H bonding. Each of the four active sites in UOx is formed by residues from two subunits and located at the subunit–subunit interface. In order to understand the origin of direct electron transfer through electrode and active site of enzyme, the surface morphology of the optimized ZnO:N (ZnO:N(08)) thin film is also investigated using SEM measurement as shown in Fig. 3(b)(i). The analysis were carried out on the top surface of the thin film and it was found that ZnO:N thin film grows on the surface of ITO/glass electrode by forming an array of vertically aligned nanorods. The grown ZnO:N nanorods are closely spaced and well isolated from each other. The formation of array of vertically aligned ZnO:N nanorods on the surface of ITO/glass electrode provides large and porous active surface area (even between the nanorods) for binding of enzyme which leads to greater and efficient uricase immobilization, with active center in contact with synthesized ZnO:N nanorods. Since, the charge transfer resistance of ZnO:N nanorod thin film is very low, it can provide a direct electron communication link from enzyme active center to the bottom conducting electrode. Thus, it is the ZnO:N nanorods with a low charge transfer resistance (*Rct*) which binds the active site of enzyme to the electrode. The detailed schematic representation of linkage of enzyme active site to the electrode for direct electron transfer is shown in Scheme 1(a). Therefore, it is inferred that N doping improves the conductivity of ZnO thin film matrix significantly which provides direct electron transmission paths through the nanorod structure between enzyme active center and bottom electrode.

It is important to note that both the formation of array of isolated nanorod structure and the high conductivity of ZnO:N thin film matrix are crucial for realizing the third generation biosensor.

In order to confirm the proposed electron transfer mechanism through electrode and active side of enzyme, two more matrices were prepared by PLD technique: (i) pure ZnO film (matrix A) as prepared on ITO/glass electrode under same processing conditions, and (ii) N doped ZnO (ZnO:N) thin film (matrix B) deposited at substrate temperature of 500 °C while keeping other growth conditions same. The morphology of pure ZnO film was found to be similar as that observed for ZnO:N film having array of vertically aligned nanorods, but value of *Rct* (1.4 kΩ) was two orders greater in magnitude than that of ZnO:N(08) thin film (30 Ω) (Fig. 3). Further, CV spectra show that pure ZnO thin film based electrode does not exhibit any redox peak in the entire measured range of sweep voltage (Fig. 4). This clearly indicates that high resistance of pure ZnO thin film provides hindrance to the transfer of electrons via nanorod structure and is not suitable for the fabrication of third generation biosensor.

Similarly, in another control experiment, the studies on ZnO:N thin film (matrix B) deposited at 500 °C is carried out. It is worth noticing that the CV spectra of bio-electrode based on matrix B as well did not give any redox peak in the measured voltage range. This may be attributed to the fact that although the value of *Rct* for matrix B was slightly lower (24 Ω), but the surface morphology was very smooth having uniformly distributed grains as shown in Fig. 3(b)(ii). Therefore, the active centers of the immobilized enzymes may not be in contact with developed matrix and external mediator is needed to complete the enzymatic reaction.

Therefore, the performed control experiments clearly highlights that both the high conductivity and nanorod structure of ZnO:N matrix are essential for fabrication of third generation biosensor as obtained in the present work. The prepared nanorod structure is easily approachable to the active site of ZnO which reduces the response time of the prepared biosensor.

3.5. Biosensing response characteristics

To identify the optimum working conditions, pH of the electrolyte solution (PBS) was varied from 6.0 to 8.0 and the corresponding CV spectra of prepared uricase/ZnO:N (08)/ITO/glass bio-electrode were recorded. The peak oxidation current was recorded as a function of pH (Fig. 4(b), inset (ii)) and was found to be maximum for neutral pH (pH 7.0) and decreasing on either sides. So, pH of the buffer solution was maintained at 7.0 in the present experiment.

In order to analyze the bioelectrocatalytical process, CV spectra were also recorded for uricase/ZnO:N(08)/ITO/ glass bio-electrode at varying scan rates from 90 mV/s to 160 mV/s as shown in Fig. 4 (b). The anodic and cathodic peak currents increased linearly as the scan rate grew from 90 to160 mV/s (inset (i); Fig. 4(b)). In addition, the anodic and cathodic peak potential exhibits a shift towards positive and negative potentials respectively (Fig. 4(b)), with increase in scan rate implying the quasi-reversibility of the system (Matharu et al., 2009). The linear relationship between the peak currents (*Ipa* or *Ipc*) and scan rate (ν) demonstrates that the electrochemical reaction of uricase immobilized on the surface of ZnO:N(08) thin film electrode is a surface controlled process (Tyagi et al., 2013).

The surface concentration of ionic species per unit area for uricase/ZnO:N(08)/ITO/glass bio-electrode is estimated using Brown-Anson model (Bard and Faulkner, 2000). The estimated value of surface concentration of electroactive uricase is found to be about 1.54×10^{-6} mol/cm^2 which is greater in comparison to the corresponding values (2.68×10^{-9} mol/cm^2) reported by other workers for uric acid biosensors (Li and Lin, 2007). The enhanced value of surface concentration of ionic species obtained in the present work confirms that the uricase/ZnO:N(08)/ITO/glass bio-electrode exhibits high enzyme loading owing to the high surface area of ZnO:N thin film besides providing conformation to

immobilized enzyme, which is further advantageous for the improved sensitivity of the developed biosensor. It may be noted that the value of surface concentration of ionic species obtained for ZnO:N(08) thin film based bio-electrode (1.54×10^{-6} mol/cm^2) is much higher than that obtained for pure ZnO thin film based bio-electrode (7.4×10^{-8} mol/cm^2) revealing that N doping is effective in increasing the electroactive sites on electrode surface and results in increased electron transport between redox species (uricase) and electrode, thus assisting direct electrochemistry of uricase.

The electrochemical sensing response of the prepared uricase/ZnO:N(08)/ITO/glass bio-electrode towards uric acid has been investigated. CV spectra were recorded for the uricase/ZnO:N (08)/ITO/glass bio-electrode with successive addition of uric acid concentrations in PBS. The physiological range of uric acid in human serum is between 0.13 and 0.46 mM (Arora et al., 2011). Thus, the concentration of uric acid (analyte) was varied from 0.05 to 1.0 mM in the PBS solution, and the obtained sensing response for ZnO:N(08) based bio-electrode is shown in Fig. 5(a). It may be observed from Fig. 5(a) that the peak oxidation current increases continuously from 1.17 mA to 2.49 mA with increase in the uric acid concentration from 0 to 1.0 mM. The immobilized uricase reacts with analyte (uric acid) and converts it into allantoin, and during re-oxidation of uricase after enzymatic reaction, electrons

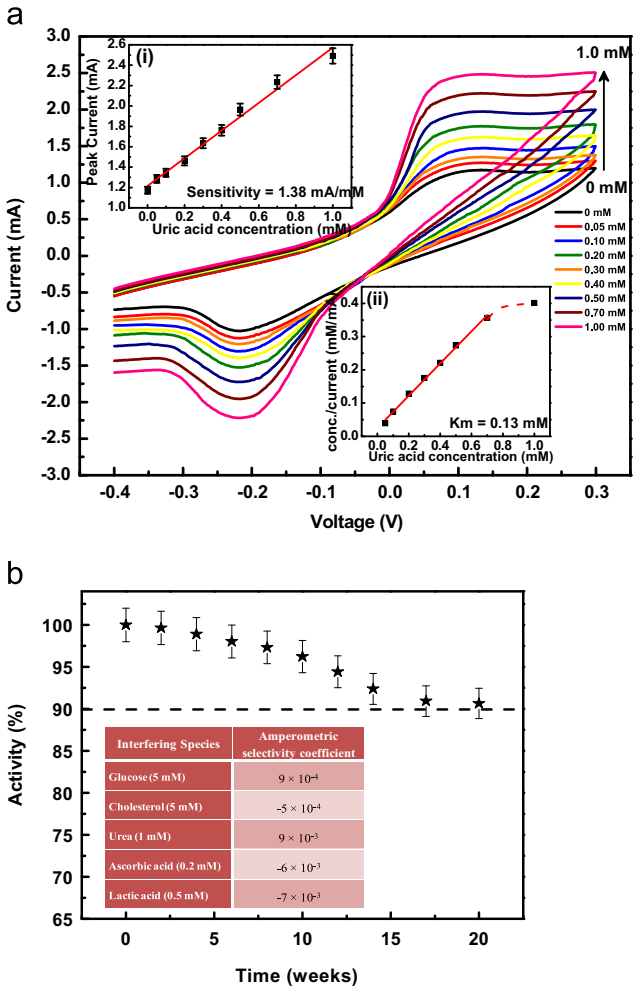

Fig. 5. (a) Sensing response of uricase/ZnO:N(08)/ITO/glass bio-electrode as a function of uric acid concentration (0.05–1.0 mM). Inset (i) gives the variation in peak oxidation current as a function of uric acid concentration and inset (ii) gives the Hanes plot; and (b) shelf life of the developed uricase/ZnO:N(08)/ITO/glass biosensor towards uric acid. Inset gives the amperometric selectivity coefficients of the developed uricase/ZnO:N/ITO/glass biosensor.

are released which are transferred directly onto the ITO electrode via the ZnO:N thin film matrix (Scheme 1(b)). The catalytic oxidation of uricase increases as the concentration of uric acid in the PBS solution increases, which thereby, results in the release of more number of electrons giving a current signal proportional to the uric acid concentration. The obtained CV responses were used to construct a calibration curve for the uricase/ZnO:N(08)/ITO/glass bio-electrode, as shown in inset (i) of Fig. 5. The inset (i) of Fig. 5(a) clearly demonstrates that the ZnO:N(08) thin film based bio-electrode exhibited good linearity for the sensing of uric acid from 0.05 mM to 1.00 mM with a correlation coefficient of 0.99. Sensitivity of the uricase/ZnO:N(08)/ITO/glass bio-electrode as calculated from the slope of the calibration curve (inset (i) of Fig. 5(a)) was found to be about 1.38 mA/mM. The lower limit of detection (LOD) was also determined and was found to be about 0.09 mM for the uricase/ZnO:N(08)/ITO/glass bio-electrode at a signal-noise ratio of 3. The obtained results clearly indicate that the sensitivity of the developed ZnO:N(08) thin film based uric acid biosensor is higher in comparison to the ones (16.60–39.35 $(\mu A)mM^{-1}$ reported in literature for other uric acid biosensors (Chen et al., 2010; Luo et al., 2006; Ahuja et al., 2010). High sensitivity of ZnO:N(08) thin film based biosensor may be due to effective immobilization of uricase having conformal orientation on the surface of ZnO:N thin film and good conductivity of ZnO:N as depicted by EIS studies which provides direct electron communication path from the enzyme active sites, thus leading to an enhancement in the electrocatalytic ability. Also, it is important to mention that the bio-electrode based on undoped ZnO thin film matrix, deposited in the similar growth conditions in the present case, is insensitive towards the uric acid in the absence of any external mediator. Thus, nitrogen doping in ZnO has proved to be a simple, reliable and efficient way to improve the sensitivity of ZnO based biosensors along with incorporating electrocatalytic properties into the matrix for the possible realization of a third generation uric acid biosensor.

In order to verify the affinity of the immobilized uricase biomolecule on the surface of ZnO:N thin film matrix, the value of Michaelis–Menten kinetic parameter (*Km*) was estimated from Hanes plot shown in the inset (ii) of Fig. 5(a). The value of *Km* was calculated from the linear region of the Hanes plot. The estimated value of *Km* is about 0.13 mM which is relatively lower than the corresponding values (0.17–7.83 mM) reported by other workers for uric acid biosensors (Zhang et al., 2007; Zhang et al., 2004; Behera and Raj, 2007; Jiang et al., 2007; Arora et al., 2009). The obtained low value of *Km* suggests that the ZnO:N (08) matrix provides a biocompatible environment and is favorable to the orientation of the immobilized uricase molecules, thereby giving the high affinity of uricase/ZnO:N(08)/ITO/glass bio-electrode towards uric acid.

Another control experiment was carried out by testing the prepared ZnO:N thin film electrode after immobilizing glucose oxidase (GOx) on the surface of nanorod thin film. GOx is an enzyme used for oxidation of glucose in our body. It is a dimeric protein that binds to β-D-glucose (an isomer of the 6 carbon sugar, glucose) and catalyzes the breaking down of sugar into metabolites. GOx catalyzes the oxidation of β-D-glucose into D-glucono-1-5-lactone which then hydrolyzes to gluconic acid. GOx requires a cofactor FAD bound deep inside the enzyme for the redox reaction. The oxidation reaction is performed by the FAD cofactors. In the GOx catalyzed redox reaction, FAD initially takes up an electron and reduces to $FADH_2$. The $FADH_2$ then oxidizes back as the electron is taken up by the molecular oxygen, as it has a higher reduction potential, which in turn reduces to H_2O_2. The active site where glucose binds is just above the FAD, in a deep pocket. It is very important to reduce the distance between the active center of GOx (FAD moiety) and the electrode in order to accomplish direct

electron transfer. Direct oxidation of glucose is reported in the literature where active site is connected to the electrode via chain of Au amino nanopartices (Sharma et al., 2012). The CV spectrum obtained for GOx/ZnO:N(08)/ITO glass bio-electrode is shown in Supplementary Fig. 4. Clear redox peaks have been observed in the CV spectra which highlights a clear possibility of sensing of glucose based on prepared ZnO:N nanorod thin film matrix. Thus, the synthesized ZnO:N nanorods connects the FAD moiety of immobilized GOx with the electrode for direct transfer of electrons. It is important to note from the CV spectra that potential window for GOx is different from that obtained for uricase which reflects that the observed peak corresponds to oxidation of enzyme and indicates the successful development of third generation biosensor. The studies based on glucose oxidase (GOx) and uricase (UOx) suggest that the prepared thin film electrode is suitable for fabrication of third generation biosensors.

3.6. Specificity of the prepared biosensor

In order to test the effect of other species present in blood which may interfere with biosensing response of uricase/ZnO:N (08)/ITO/glass bio-electrode, the interfering species including glucose (5 mM), cholesterol (5 mM), urea (1 mM), ascorbic acid (0.2 mM) and lactic acid (0.5 mM) were added in the presence of 0.3 mM uric acid and the corresponding CV spectra were recorded. Concentrations of different species are chosen on the basis of their normal concentration in human blood. Selectivity coefficients K_{sel}, were determined for the same potential that was used for the determination of calibration curve for uric acid (corresponding to peak oxidation current) using the equation (Staden et al., 2012)

$$K_{i,j}=\left(\frac{\Delta I_t}{\Delta I_i}-1\right)\times\frac{C_i}{C_j}$$

where $\Delta I_t=I_t-I_b$ and $\Delta I_i=I_i-I_b$, I_t is value of the current recorded for the mixed PBS solution having uric acid and interfering species, I_i is the value of current recorded for only uric acid (0.3 mM), I_b is the corresponding current recorded for the blank PBS solution (without analyte) and c_i and c_j are the concentrations of uric acid and interfering species, respectively in PBS solution. The values of selectivity coefficient obtained for the various interferents are listed in Fig. 5(b); inset. All values of selectivity coefficient being of the order of 10^{-3} or less (Fig. 5(b); inset) highlights that none of the tested species interfere with the measured biosensing response towards uric acid (Chachulski and Ge˛bicki, 2006). Thus, the designed uricase/ZnO:N/ITO/glass biosensor is highly selective towards the amperometric determination of uric acid without any mediator.

3.7. Stability of the biosensor

The long term stability of the prepared uric acid biosensor is investigated over a period of 5 months by measuring the electrochemical current response after regular intervals of time (15 days). The test concentration of uric acid in the stability study is kept fixed at 0.30 mM and the current is normalized with the peak current obtained when the biosensor is used for the first time. The degradation of bio-electrode is studied with respect to the deviation from this current as a function of time when the biosensor is stored for some long duration. Fig. 5(b) gives the variation in the activity of ZnO:N(08) thin film based bio-electrode as a function of time. It is observed that the biosensor retains more than 90% of its activity even after18 weeks (Fig. 5(b)) when stored at 4 °C, demonstrating the high shelf life of the developed ZnO:N (08) based bio-electrode. The shelf life of the biosensor is found to be much higher than the corresponding reports available on other bio-electrodes developed for uric acid biosensing (10–60 days) (Zhang et al., 2007; Zhang et al., 2010; Li and Lin, 2007; Luo et al., 2006; Ahuja et al., 2010; Arora et al., 2009; Hoshi et al., 2003; Kan et al., 2004; He et al., 2007; Ali et al., 2011). The high shelf life of the prepared bio-electrode may be attributed to the high stability and excellent biological compatibility of the nitrogen doped ZnO thin film matrix grown by reproducible pulsed laser deposition technique (PLD) which provides good microenvironment to the enzyme to maintain its activity.

4. Conclusions and outlook

A novel third generation uric acid biosensor based on the direct transfer of electron from the immobilized enzyme onto the electrode is developed. The doping of N at O site in ZnO lattice induces the electrocatalytic functionality besides providing the conformation to the immobilized uricase. The prepared uricase/ZnO:N(08)/ITO/glass bio-electrode exhibits enhanced sensitivity (1.38 mA(mM)$^{-1}$) and good linearity over a wide detection range (0.05–1.0 mM) of uric acid in the absence of any mediator. The low *Km* value of 0.13 mM indicates high affinity of the immobilized uricase on the surface of ZnO:N thin film towards uric acid. The ZnO:N (8% N doped) thin film based uric acid biosensor exhibits remarkably high stability with a shelf-life of more than 18 weeks. It is inferred that nitrogen doped ZnO has higher electrical conductivity and better electron communication feature than the undoped ZnO matrix and is extremely attractive for realization of efficient third generation biosensors.

Acknowledgments

Authors are thankful to Department of Science and Technology (DST), India for financial assistantship. One of the authors (K.J) is also thankful to UGC and University of Delhi for research fellowship.

Appendix A. Supplementary materials

Supplementary data associated with this article can be found in the online version at http://dx.doi.org/10.1016/j.bios.2013.11.015.

References

Ahmad, R., Tripathy, N., Kim, J.H., Hahn, Y.B., 2012. Sens. Actuators B 174, 195.
Ahuja, T., Rajesh, Kumar, D., Tanwar, V.K., Sharma, V., Biradar, A.M., Singh, N., 2010. Thin Solid Films 519, 1128.
Ali, S.M.U., Alvi, N.H., Ibupoto, Z., Nur, O., Willandera, M., Danielsson, B., 2011. Sens. Actuators B 152, 241.
Arora, J., Nandwani, S., Bhambi, M., Pundir, C.S., 2009. Anal. Chim. Acta 647, 195.
Arora, K., Tomar, M., Gupta, V., 2011. Biosens. Bioelectron. 30, 333.
Bard, A.J., Faulkner, L.R., 2000. Electrochemical Methods: Fundamentals and Applications, second ed. Wiley, New York.
Batra, N., Tomar, M., Gupta, V., 2012. Analyst 137, 5854.
Behera, S., Raj, C.R., 2007. Biosens. Bioelectron. 23, 556.
Cao, Z., Jiang, X., Xie, Q., Yao, S., 2008. Biosens. Bioelectron. 24, 222.
Chachulski, B., Ge˛bicki, J., 2006. Electroanalysis 18, 433.
Chen, P.Y., Vittal, R., Nien, P.C., Liou, G.S., Ho, K.C., 2010. Talanta 80, 1145.
Dai, Z., Shao, G., Hong, J., Bao, J., Shen, J., 2009. Biosens. Bioelectron. 24, 1286.
Das, M., Sumana, G., Nagarajan, R., Malhotra, B.D., 2010. Appl. Phys. Lett. 96, 133703.
Devi, R., Thakur, M., Pundir, C.S., 2011. Biosens. Bioelectron. 26, 3420.
Djuriši ć, A.B., Leung, Y.H., Tam, K.H., Ding, L., Ge, W.K., Chen, H.Y., Gwo, S., 2006. Appl. Phys. Lett. 88, 103107.
Dominici, L., Maur, M.A., Michelotti, F., 2012. J. Appl. Phys. 112, 053514.
Fatemi, H., Khodadadi, A.A., Firooz, A.A., Mortazavi, Y., 2012. Curr. Appl. Phys. 12, 1033.
Game, O., Singh, U., Gupta, A.A., Suryawanshi, A., Banpurkar, A., Ogale, S., 2012. J. Mater. Chem. 22, 17302.
Gao, J.Y., Qin, R., Luo, G.F., Lu, J., Wang, Y.L., Ye, H.Q., Liao, Z.M., Zhao, Q., Yu, D.P., 2010. Phys. Lett. A 374, 3546.
Guo, C., Sun, H., Zhao, X.S., 2012. Sens. Actuators B 164, 82.
Gupta, V., Mansingh, A., 1996. J. Appl. Phys. 80, 1063.

He, J.B., Jin, G.P., Chen, Q.Z., Wang, Y., 2007. Anal. Chim. Acta 585, 337.
Hoshi, T., Saiki, H., Anzai, J., 2003. Talanta 61, 363.
Jiang, Y., Wang, A., Kan, J., 2007. Sens. Actuators B 124, 529.
Jindal, K., Tomar, M., Gupta, V., 2012. J. Appl. Phys. 111, 102805.
Kan, J., Pan, X., Chen, C., 2004. Biosens. Bioelectron. 19, 1635.
Kong, T., Chen, Y., Ye, Y., Zhang, K., Wang, Z., Wang, X., 2009. Sens. Actuators B 138, 344.
Li, J., Lin, X.Q., 2007. Anal. Chim. Acta 596, 222.
Li, P., Deng, S.H., Li, Y.B., Zhang, L., Liu, G.H., Huang, J., 2012. Chin. J. Chem. Phys. 25, 48–52.
Liu, L., Xu, J., Wang, D., Jiang, M., Wang, S., Li, B., Zhang, Z., Zhao, D., Shan, C.X., Yao, B., Shen, D.Z., 2012. Phys. Rev. Lett. 108, 215501.
Lu, X., Zhang, H., Ni, Y., Zhang, Q., Chen, J., 2008. Biosens. Bioelectron. 24, 93.
Luo, Y.C., Do, J.S., Liu, C., 2006. Biosens. Bioelectron. 22, 482.
Matharu, Z., Pandey, P., Pandey, M.K., Gupta, V., Malhotra, B.D., 2009. Electroanalysis 14, 1587.
Mehan, N., Gupta, V., Sreenivas, K., Mansingh, A., 2004. J. Appl. Phys. 96, 3134.
Menon, R., Gupta, V., Tan, H.H., Sreenivas, K., Jagadish, C., 2011. J. Appl. Phys. 109, 064905.
Niu, S., Han, B., Cao, W., Zhang, S., 2009. Anal. Chim. Acta 651, 42.
Panigrahy, B., Aslam, M., Misra, D.S., Ghosh, M., Bahadur, D., 2010. Adv. Funct. Mater. 20, 1161.
Pundir, C.S., Chauhan, N., Verma, Rajneesh, Ravi, M., 2011. Sens. Actuators B 155, 796.
Saha, S., Arya, S.K., Singh, S.P., Sreenivas, K., Malhotra, B.D., Gupta, V., 2009. Anal. Chim. Acta 653, 212.
Saha, S., Gupta, V., 2011. J. Appl. Phys. 110, 064904.
Sharma, S., Gupta, N., Srivastava, S., 2012. Biosens. Bioelectron. 37, 30–37.
Staden, R.S., Nejem, R.M., Staden, J.F., Aboul-Enein, H.Y., 2012. Biosens. Bioelectron. 35, 439.
Tomar, M., Gupta, V., Sreenivas, K., Mansingh, A., 2005. IEEE Trans. Device Mater. Reliab. 5, 494.
Tyagi, M., Tomar, M., Gupta, V., 2013. Biosens. Bioelectron. 41, 110.
Wang, C., Tan, X., Chen, S., Yuan, R., Hu, F., Yuan, D., Xiang, Y., 2012. Talanta 94, 263.
Wang, J., Li, S., Zhang, Y., 2010. Electrochim. Acta 55, 4436.
Wei, Y., Li, Y., Liu, X., Xian, Y., Shi, G., Jin, L., 2010. Biosens. Bioelectron. 26, 275.
Wu, K., Fang, Q., Wang, W., Thomas, M.A., Cui, J., 2012. J. Appl. Phys. 111, 063530.
Wu, K.Y., Fang, Q.Q., Wang, W.N., Zhou, C., Huang, W.J., Li, J.G., Lv, Q.R., Liu, Y.M., Zhang, Q.P., Zhang, H.M., 2010. J. Appl. Phys. 108, 063530.
Xiang, C., Zou, Y., Sun, L.X., Xu, F., 2009. Sens. Actuators B 136, 158.
Yadav, H.K., Gupta, V., 2012. J. Appl. Phys. 111, 102809.
Yadav, H.K., Katiyar, R.S., Gupta, V., 2012. Appl. Phys. Lett. 100, 051906.
Yadav, H.K., Sreenivas, K., Katiyar, R.S., Gupta, V., 2007. J. Phys. D: Appl. Phys. 40, 6005.
Yadav, S., Devi, R., Kumar, A., Pundir, C.S., 2011. Biosens. Bioelectron. 28, 64.
Yin, H., Ai, S., Shi, W., Zhu, L., 2009. Sens. Actuators B 137, 747.
Zeng, H., Duan, G., Li, Y., Yang, S., Xu, X., Cai, W., 2010. Adv. Funct. Mater. 20, 561.
Zhang, C., Wang, G., Ji, Y., Liu, M., Feng, Y., Zhang, Z., Fang, B., 2010. Sens. Actuators B 150, 247.
Zhang, F., Wang, X., Ai, S., Sun, Z., Wan, Q., Zhu, Z., Xian, Y., Jin, L., Yamamoto, K., 2004. Anal. Chim. Acta 519, 155.
Zhang, Y., Wen, G., Zhou, Y., Shuang, S., Dong, C., Choi, M.M.F., 2007. Biosens. Bioelectron. 22, 1791.